DEVELOPMENTS IN MODELLING AND SIMULATION..JAPAN, SOUTH KOREA AND CHINA

Prediction for cryogenic formability of AA2219 alloy cylindrical parts with friction stir weld

Wei Liu[1,2] · Yonggang Hao[1,2] · Wen Sun[1,2] · Mengjia Yao[1,2]

Abstract

A cryogenic deep drawing process was proposed for complex curved surface part forming with aluminum alloy friction stir welded (FSW) blanks. The experimental forming limit curves (FLCs) of AA2219 alloy FSW blanks were obtained using the Nakajima tests at -196 °C. The theoretical FLC of base metal (BM) and weld zone for the FSW blank were calculated by M-K theory, respectively. The limited drawing ratio (LDR) was tested by the deep drawing of the hemispherical bottom cylindrical parts, and the splitting behavior of the drawn-part at ultra-low temperature was accurately predicted using the numerical simulations combined with theoretical FLCs. It was found that the forming limits and LDR of the FSW blanks were improved at -196 °C, and the FLD_0 and LDR reached to 0.27 and 1.90, respectively. The improved cryogenic deep drawability was attributed to hyper hardening and high plasticity of the FSW blanks, which help to transfer deformation and prevent localized deformation from splitting in weak deformation zone. Finally, three effective methods were further proposed to improve cryogenic formability of FSW blanks. The increased blank holder force can ensure the suppressed co-existence of wrinkling and splitting due to increased resistance to localized deformation ability during cryogenic deep drawing. The strain distribution between the weld and BM zone of the deep drawn parts was more uniform by isothermal condition. Furthermore, the cryogenic formability can be further improved for the FSW blank with an offset weld.

Keywords Hemispherical bottom cylindrical parts · Cryogenic deep drawing · FLC · LDR · M-K theory · Fracture prediction

Nomenclature

f_0	Initial thickness unevenness
$\bar{\varepsilon}$	Equivalent plastic strain
ε_{2b}	Minor strain of weaker zone
σ_{1b}	Major stress of weaker zone
$\Delta\varepsilon_{1a}$	Major strain increment of stronger zone
ρ	Strain ratio
K	Strength coefficient
r_0, r_{45}, r_{90}	Lankford coefficient
φ	Effective stress increment divided by major stress increment
F, G, H, N	Coefficient of Hill's 1948 yield function
β	Effective strain increment divided by major strain
$\bar{\sigma}$	Equivalent stress
ε_{2a}	Minor strain of stronger zone
σ_{1a}	Major stress of stronger zone
ε_3	Normal strain
D_0	Initial blank diameter
α	Stress ratio
n	Strain hardening exponent
$\bar{r}$	True plastic strain ratio

✉ Wei Liu
liuw@hit.edu.cn

1 National Key Laboratory for Precision Hot Processing of Metals, Harbin Institute of Technology, 150001 Harbin, China

2 School of Materials Science and Engineering, Harbin Institute of Technology, 150001 Harbin, China

Introduction

With the development of the aerospace industry, the large-scale thin-walled curved parts of high-strength aluminum alloy are widely used in the rockets and aircraft. These components deformed by tailor welded blanks have been adopted due to the limited size of blanks instead of multi-pieces

welded component. However, the complex components of FSW blank faced with more challenges for forming and manufacturing because of the strong heterogeneity of the material and geometry introduced by welds [1–4]. The forming limits of FSW blanks were low at room temperature (RT), and hot forming will lead to uneven deformation, local thinning and abnormal grains growth of welds. The different attempts were also applied to improve the formability of aluminum tailor welded blanks produced by the FSW [5], including post-weld heat-treatment, optimizing welding parameters and so on. However, the properties improvement of FSW blanks was not obvious. Recently, a promising cryogenic forming technique was regarded as a green and efficient process to improve the formability, which has been paid more and more attentions [6–8].

It is of great significance to evaluate and predict cryogenic formability of the FSW blanks. The FLC is regard as an important method to evaluate the formability [9–12]. At present, there have been some researches on cryogenic FLCs by experiments and theoretical predictions of aluminum alloys. It was found that the improved hardening ability for face-centered cubic aluminum at ultra-low temperatures lead to a significant increase in the forming limits, and the forming limits in the plane strain state was improved obviously [13]. In addition, in order to apply cryogenic characteristics to practical forming processes, the influence of cryogenic temperatures on the formability of aluminum in stretching, deep drawing and hole flanging were studied firstly. Recently, Yi et al. studied the cryogenic forming limit curves of 2024-O alloy by experiments and theoretical calculations, and found that the lower the temperature, the higher the forming limits and the better the formability [14]. They brought the constitutive equation into the M–K model for cryogenic FLC prediction, studied the impact of different yield functions and different temperatures on the prediction results, and compared them with the experimental results. A novel testing method for analyzing formability at low temperatures incorporating a newly-designed digital image correlation testing device was developed by Yuan et al., and they found that the FLD_0 of AA2219 alloy with solution treatment increased from 0.23 of RT to 0.32 at -196 °C [15]. Moreover, the LDR of the cylindrical parts also can be used to evaluate the cryogenic formability of the blanks. At -196 °C, the LDR of the solution treated AA2219 alloy increased from 1.8 at RT to 2.08 [16], and the proposed cryogenic deep drawing process and newly-designed forming system can be adopted to overcome the disadvantages when forming aluminum alloy deep-drawn components with complex shapes at room or high temperatures. Schneider R et al. found that the LDR of flat-bottomed cylindrical parts of EN AW-5182-H111 and EN AW-6016-T4 also increased from room temperature to -196 °C. The former LDR increased from 2.0 to 2.2, and the latter of LDR reached to 2.1 [17].

According to above researches, the FLCs and LDR of the homogeneous blank at ultra-low temperature were significantly improved, however, the cryogenic FLC and LDR of FSW blanks were still not reported to our knowledge. Concerning FSW blanks, two approaches can be used to obtain the FLC. The first approach combined properties of the BM and the weld zone, and provided only a FLC representing the whole blank. The second approach provided various FLCs for the BM and the weld zone [18]. Since there can be a considerable difference between the forming limits of the BM and weld zone, the FLC obtained by the later was more accurate. Generally, the experiments have can only obtain a limited points of curves. Therefore, the theoretical prediction methods have become the focus of FLC research. The groove instability theory proposed by the M–K model [7, 19], is the most widely used FLC prediction theory [20–22]. However, preexisting research mainly focuses on the prediction of FLC at room and high temperatures. Although the cryogenic FLC of homogeneous blank was studied [13, 14], there is a lack of prediction research on FLC for the heterogeneous blank at cryogenic temperatures.

Therefore, in this study, the cryogenic FLCs of FSW blanks was obtained by the experiments and M-K theoretical calculation. Deformation paths of typical positions under different strain states of the weld zone were analyzed, and both the forming limits and the LDR of FSW blanks were studied at ultra-low temperature. The cryogenic formability and the effect of deep drawing parameters on hemispherical bottom cylindrical parts were predicted systematically by the simulations. The mechanism of improved cryogenic deep drawability was analyzed, and the effective methods to improve the cryogenic formability were also proposed finally.

Materials and experimental methods

The FSW blanks preparation and tensile tests

The experimental material is 2219-O aluminum alloy FSW blanks with a thickness of 2.0 mm. Figure 1a and b show the preparation process of FSW blanks and dimensions of pin tool. The tool shoulder diameter is 10 mm, with pin height, and minimum diameter being respectively 1.85 mm and 1 mm. The tilt angle is fixed to 2º and the plunge depth is 0.5 mm. The rolling direction was perpendicular to the weld direction. The welding parameters were used in a rotational rate of 800 rpm and a welding speed of 200 mm/min. Based on the assumption that the weld zone is an isotropic homogeneous material [23–25], the uniaxial tensile properties of the BM zone and the longitudinal weld (LW) zone were carried out with the specimen size of a 30 mm gauge length and 10 mm gauge width according to the GB/T 2651−2008

Fig. 1 The FSW blanks preparation, configuration (**a**, **b**) for tensile tests (**c**) and microstructures of the joints (**d**)
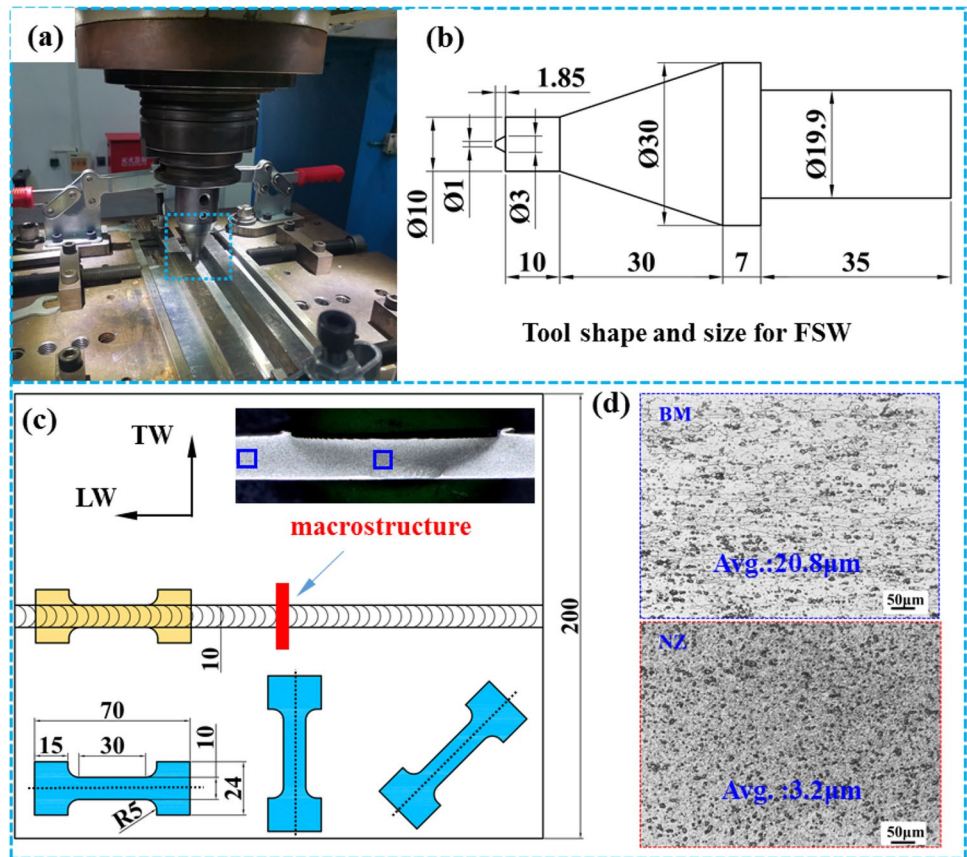
standard. Dimensions and locations for the tensile specimen are shown in Fig. 1c. The average grain size of the BM was 20.8 µm and the nugget zone (NZ) was about 3.2 µm as shown in Fig. 1d. The weld bead across the section shows a region of large deformation, which shows a very fine equiaxed grain structure.

Figure 2a shows the tension experimental details with the cryogenic chamber. Temperature ranges from LN_2 to RT were obtained by using a mixture of LN_2 and air, and the LN_2 flow rate was controlled programmatically through a solenoid valve. Figure 2b show the time-dependent curves of the specimen center temperature during tension at different temperatures.

The Nakajima tests

Figure 3a shows the schematic diagram of the Nakajima tests devices, and the punch radius is 25 mm. The blank was immersed in LN_2 for 10 min to ensure the uniform temperature, and then the cryogenic stretching forming

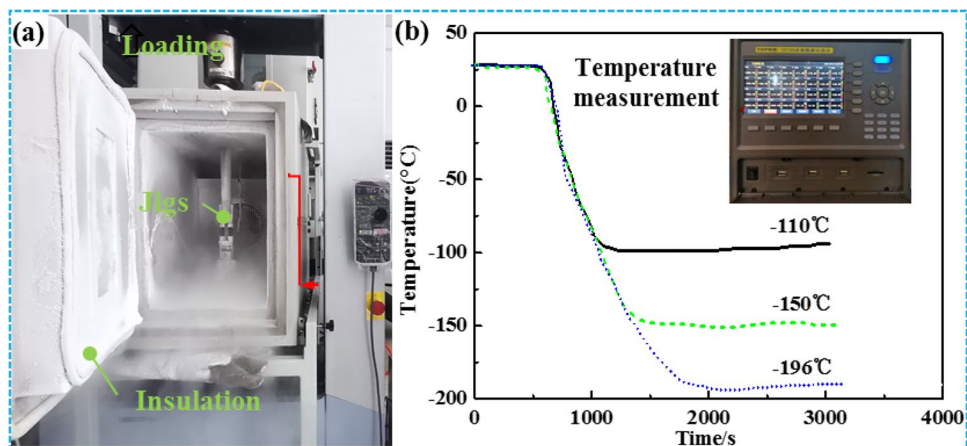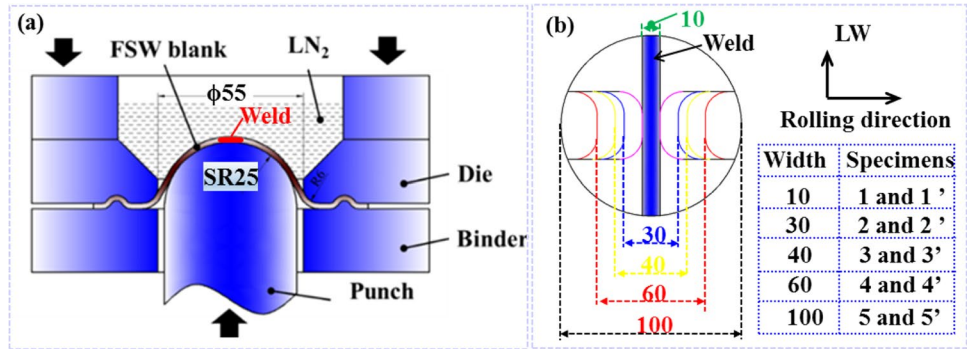**Fig. 2** Tensile test setup (**a**) and temperature control curves (**b**)

Fig. 3 Schematic diagram of the Nakajima testing devices and the geometry and dimensions (in mm) of the specimen design for formability evaluation (the numbers from 1 to 5 were tested at RT, and the numbers from 1' to 5' were tested at -196 °C)

were conducted. At present, there is no standard for the FLC tests of tailor-welded blanks. The FLCs test samples of FSW blanks were designed with reference to the GB/T 24171.2–2009, as shown in Fig. 3b. Weld orientation and location can significantly affect the forming limit of the FSW blanks [26, 27]. In this paper, the weld direction was parallel with the direction of the parallel section of the sample. The major strain direction of the weld zone was consistent with the weld direction during the loading process, which can reflect the formability of the weld zone under terrible strain conditions [28, 29] The ARGUS technology (GOM, Germany) was used to determine the limit strains at the onset of localized necking in the Nakajima tests. Before testing, the waisted specimens were marked using electrochemical etching with square arrays of circular white dots of 1 mm diameter and 2 mm center-to-center distance. In addition, the bulging experiment at LN_2 temperature, that is -196 °C, can be carried out by immersing in LN_2 to maintain stable temperature. Moreover, the FSW blank will have more significant "dual enhancement effect" of strength and plasticity below a critical temperature. Therefore, the experimental FLCs at RT and the lowest achievable temperature − 196 °C

were conducted to compare the formability difference of the FSW blanks.

Hemispherical bottom cylindrical parts deep drawing

Figure 4 shows the cryogenic deep drawing devices and finite element model of the hemispherical bottom cylindrical part forming. The outer diameter of the deep drawing punch is 100 mm. The inner diameter of the die is 105 mm, and the fillet radius of the die is 10 mm. The experiments and numerical simulations were carried out to study the LDR of cylindrical parts at RT and ultra-low temperatures. The Poly Tetra fluoroethylene (PTFE) was used to lubricate the punch and FSW blanks during the forming at room and cryogenic temperature. Numerical simulations were used to obtain the strain paths at different positions in the weld zone during the deep drawing process. The weld zone and the BM zone were established for the FE model, and different material parameters were assigned as shown in Table 1, respectively. Setting the two zones as a "component set" ensured that the seamless mesh between the weld and the BM was
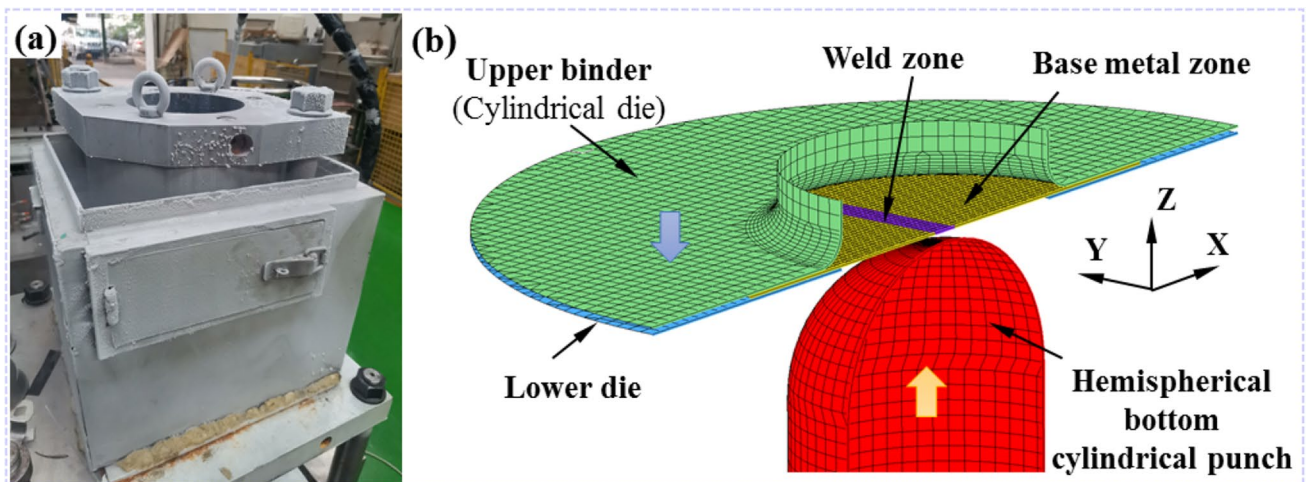

Fig. 4 Cylindrical parts deep drawing process: experimental setup (**a**), a half symmetric FE model (**b**)

Table 1 Finite element model parameters

| Parameters	Values		Material type	Yield criterion
Mesh type of blank	Shell, Belytschko-Tsay			
Mesh type for punch, die and blank holder	Shell, Belytschko-Tsay			
Size of mesh	2 mm			
Material model	Zone		Material type	Yield criterion
	Weld zone		#MAT 024	Von Mise
	Base metal		#MAT 037	Hill'1948
	Punch, blank holder, die		#MAT 020	Rigid body
Type of contact	Contact_forming_one_way_surface_to_surface			
Boundary conditions	The weld and base metal zone are set as one part set			
	Z-translational degrees-of-freedom by defined curve for punch			
Friction coefficient	0.2			
Type of solver	LS-DYNA_SMP_S_R11			
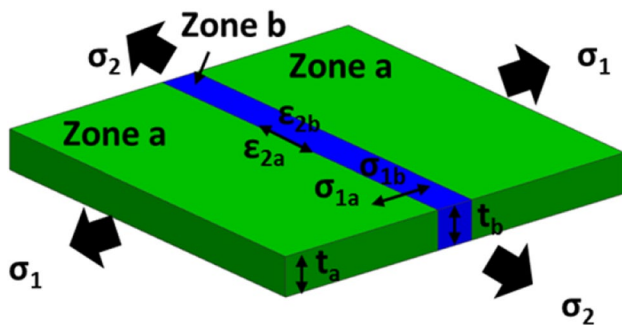
Fig. 5 Schematic diagram of the M-K model

participated in deformation at the same time. In addition, the Hill'48 yield criterion was used in the BM zone [15], and the isotropic von Mises yield criterion was used in the weld zone. The hardening criterion all adopt Hollomon equation, and its expression is:

$$\bar{\sigma} = K\bar{\varepsilon}^n \tag{1}$$

where $\bar{\sigma}$ is the equivalent stress, $\bar{\varepsilon}$ is the equivalent plastic strain, n is the hardening exponent, K is the strength parameter. In addition, the punch speed in the experimental tests and numerical simulation both were 1 mm/s. The kinetic energy of the alloy for the quasi-static forming was not exceed 5% of its internal energy throughout most of the process.

Theoretical calculation of FLCs

The theoretical analysis of the FLCs of the weld zone and BM zone were carried out by using the M-K model, respectively. The model assumed that there are defects in the initial state of the material in BM or weld zone, as shown in Fig. 5.

The material defects are represented by the initial thickness unevenness $f_0 = t_{b0}/t_{a0}$. The "b" represents the weaker zone due to the defects. For example, during the loading process, as the strain increased in the BM zone, the initial defects existing continued to expand, and the alloy was destroyed finally due to the defects expand rapidly [30, 31].

During the deformation process, the stress and strain of stronger zone "a" and weaker zone "b" satisfy the coordination relationship. The strain is equal in direction of parallel weaker zone, namely

$$\varepsilon_{2a} = \varepsilon_{2b} \tag{2}$$

According to the force equilibrium condition, the force in the perpendicular weaker zone direction can be given by,

$$\sigma_{1a}t_a = \sigma_{1b}t_b \tag{3}$$

The strain along the thickness direction is $\varepsilon_3 = \ln(t/t_0)$. The hardening law satisfied the Eq. (1), Eq. (3) can be transformed as

$$\frac{1}{\varphi_a}\bar{\varepsilon}_a^n = f_0 \exp(\varepsilon_{3b} - \varepsilon_{3a})(\frac{1}{\varphi_b})\bar{\varepsilon}_b^n \tag{4}$$

φ is the effective stress increment divided by major stress increment, which can be calculated by the stress ratio α for the isotropic weld zone by Eq. (5).

$$\varphi = \frac{\bar{\sigma}}{\sigma_1} = \sqrt{1 + \alpha^2 - \alpha} \tag{5}$$

$$\alpha = \frac{\sigma_2}{\sigma_1} \tag{6}$$

In addition, according to incremental theory and plastic work principle, the following parameters can be calculated. ρ is defined as minor strain increment divided by major strain

increment, β is the effective strain increment divided by major strain increment, and they are described as follows:

$$\rho = \frac{d\varepsilon_2}{d\varepsilon_1} = \frac{2\alpha - 1}{2 - \alpha} \tag{7}$$

$$\beta = \frac{d\bar{\varepsilon}}{d\varepsilon_1} = \frac{2\varphi}{2 - \alpha} \tag{8}$$

For the BM zone, according to the Hill'1948 yield criterion [32], the φ and ρ can be obtained by the Eqs. (9) and (10), respectively.

$$\varphi = \sqrt{\frac{[\bar{r}(1 - \alpha)^2 + \alpha^2 + 1]}{\bar{r} + 1}} \tag{9}$$

$$\rho = \frac{\alpha - \bar{r}(1 - \alpha)}{1 + \bar{r}(1 - \alpha)} \tag{10}$$

The computation process of M-K model can be simplified to the function of $\bar{\varepsilon}_a, \bar{\varepsilon}_b, \varepsilon_{3b}, \varepsilon_{3a}, \alpha_a, \Delta\varepsilon_{1a}$ and $\Delta\varepsilon_{1b}$. It is assumed that the major strain in region "a" increases by step length of $\Delta\varepsilon_{1a} = 0.005$. $\Delta\bar{\varepsilon}_a$ can be obtained as shown in Fig. 6. The material property parameters and a certain stress ratio are substituted into the computation program of M-K model, and then the equivalent strain increment for "b" region ($\Delta\bar{\varepsilon}_b$) can be obtained. When the major strain ratio between the strong zone and weaker zone satisfies the Eq. (11), the material is unstable, and the forming limit strain of the BM zone can be obtained with changing α_a in the range of 0 ~ 1. In this study, the forming limit is assumed to achieve when the ratio of the equivalent strain increments of weaker zone to those of the stronger zone is larger than 10 as shown in Fig. 6. The FLC of weld zone also can be obtained by similar method. The obtained FLCs were used in the simulations to predict the splitting during the cryogenic forming.

$$\frac{\varphi_b}{\varphi_a}(\bar{\varepsilon}_a + \Delta\bar{\varepsilon}_a)^n = f_0 \exp(\varepsilon_{3b} - \varepsilon_{3a} + \Delta\varepsilon_{3b} - \Delta\varepsilon_{3a})(\bar{\varepsilon}_b + \Delta\bar{\varepsilon}_b)^n \tag{11}$$

$$\frac{\Delta\bar{\varepsilon}_b}{\Delta\bar{\varepsilon}_a} \geqslant 10 \tag{12}$$

Results and discussion

Tensile mechanical properties of weld and BM zone

Figure 7 shows the tensile true stress - strain curves of longitudinal weld (LW) and BM (in the longitudinal direction) at different temperatures. Table 2 shows the tensile mechanical properties and Hollomon parameters.
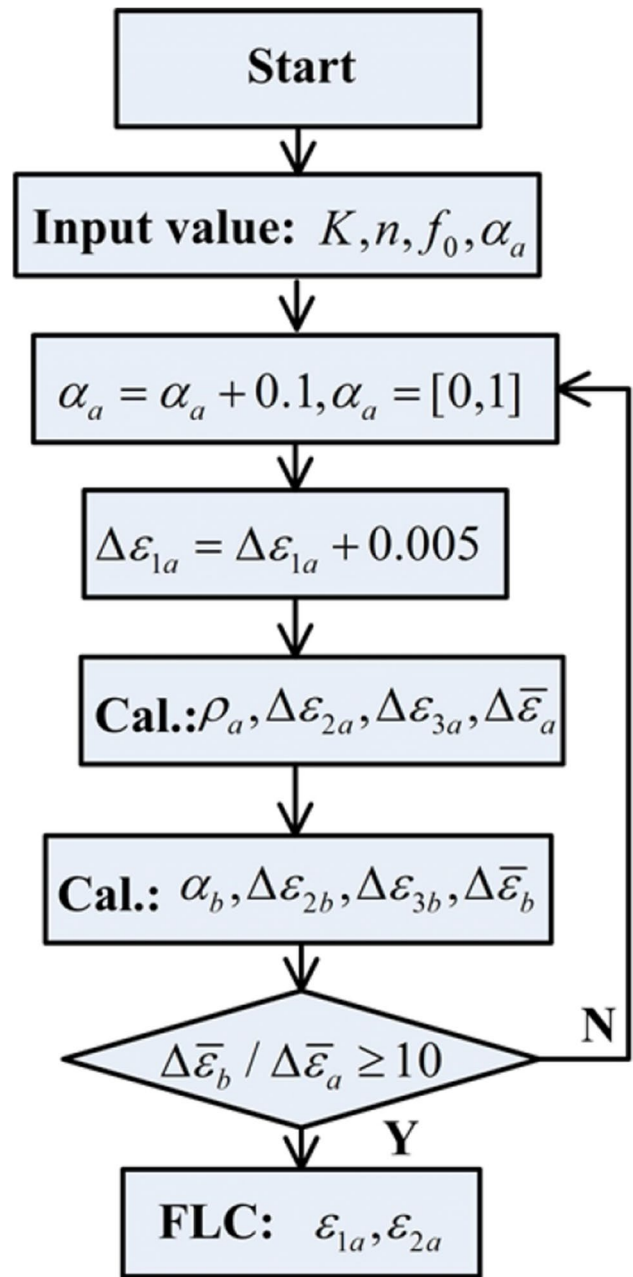

Fig. 6 The flow chart of predicting cryogenic FLC of BM or weld zone based on M-K model

It was found that both the BM and the weld zone exhibited a "dual enhancement effect" of strength and plasticity with decreasing temperatures. The elongation after fracture of the BM zone increased from 27.8 to 40.7% and an increase of 46.4% from RT to -196 °C. The hardening exponent n increased from 0.33 to 0.46 and by 39.4%. In the weld zone, the elongation after fracture increased from 21.8 to 28.5% and the hardening exponent increased from 0.29 to 0.44, which increased by 30.3% and 51.7%, respectively. At -196 °C, the strength coefficient of the

BM increased to the same level as that of the weld, and the BM zone was significantly strengthened. At the same temperature, the strength of the weld zone was higher than that of the BM zone, and the plasticity was lower. The increased strength of AA2219 alloy at ultra-low temperature was mainly related to the significant dislocation strengthening, and the plasticity improvement was due to the inhibition of local planar slip and the occurrence of multiple slips [33]. The mechanical properties of weld zone and BM zone were quite different due to different heat flow and plastic strain during friction stir processing [34, 35]. The difference in mechanical properties was related to the different grain size, as shown in Fig. 1d. Figure 8 shows that the strength difference between weld zone and BM zone decreased significantly at -196 °C, which was ascribed to the more significant strengthening of BM zone with coarse grain [36].

Table 3 shows the material model of the anisotropy coefficient r for the BM zone and the Hill'48 yield criterion parameters obtained by uniaxial tension. The weighted average anisotropy coefficients $\bar{r}$ at -196 °C increased from 0.497 to 0.575. These obtained parameters were used in simulations of RT and cryogenic deep drawing.

Fig. 7 Hollomon curve fitting with experimental true stress-strain curve at different temperatures for the LW (**a**) and BM zone (**b**)
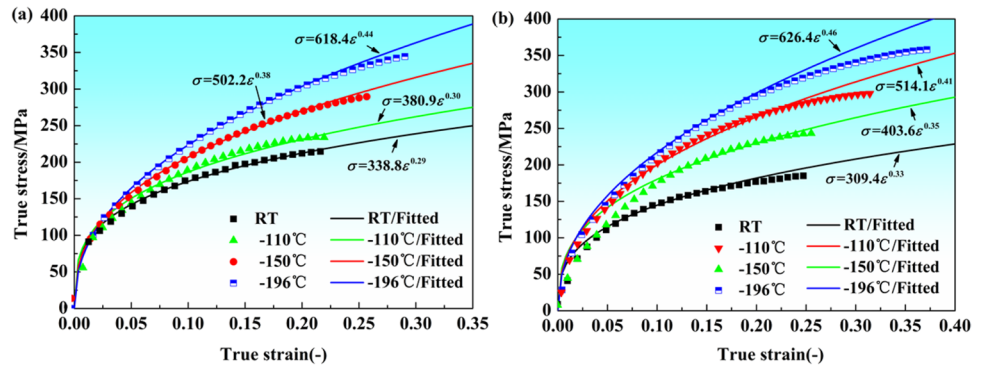

Table 2 Mechanical properties of the LW and BM zone in different conditions

	Temperature	YS/MPa	UTS/MPa	ELs after fracture/%	Hardening exponent/n	Strength coefficient /K	R^2
BM	RT	59.6	144.9	27.8	0.33	309.4	0.995
	-110 °C	67.1	189.5	28.6	0.35	403.6	0.988
	-150 °C	72.5	221.8	33.2	0.43	514.1	0.994
	-196 °C	85.5	252.1	40.7	0.46	626.4	0.987
LW	RT	92.3	172.9	21.8	0.29	338.79	0.994
	-110 °C	97.3	190.6	22.7	0.30	380.96	0.993
	-150 °C	109.1	224.1	24.9	0.38	502.15	0.998
	-196 °C	113.3	258.4	28.5	0.44	618.42	0.999

Where, YS = yield strength, UTS = ultimate tensile strength, EL = elongation after fracture

Fig. 8 Comparisons of tensile curves for weld and BM zone (**a**) and strength difference (**b**) at RT and − 196 °C (CT)
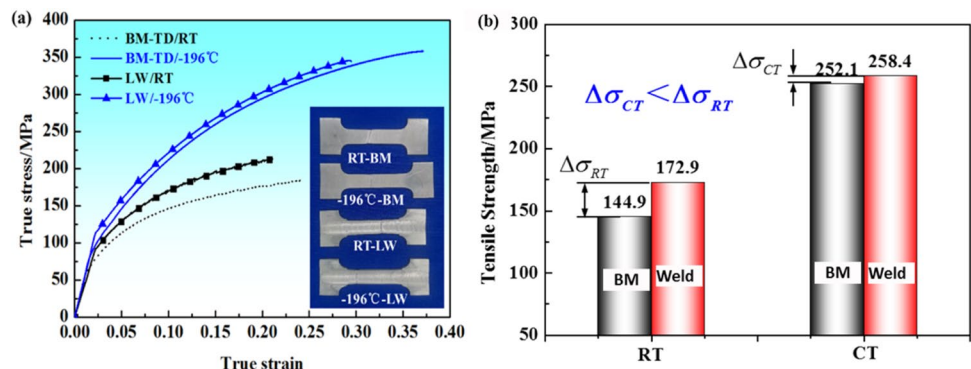
Table 3 Anisotropic parameters and Hill'48 model of the BM tested in RT and −196 °C

Parameter	r_0	r_{45}	r_{90}	$\bar{r}$	Hill'48 yield model parameters			
					F	G	H	N
RT	0.382	0.671	0.264	0.497	1.05	0.723	0.276	2.075
-196℃	0.432	0.812	0.244	0.575	1.236	0.698	0.302	2.555

Where r_0, r_{45}, and r_{90} are anisotropy value along rolling, diagonal, and transverse direction respectively

Fig. 9 Formed samples after failure in hemispherical punch bulging tests at RT and −196 °C
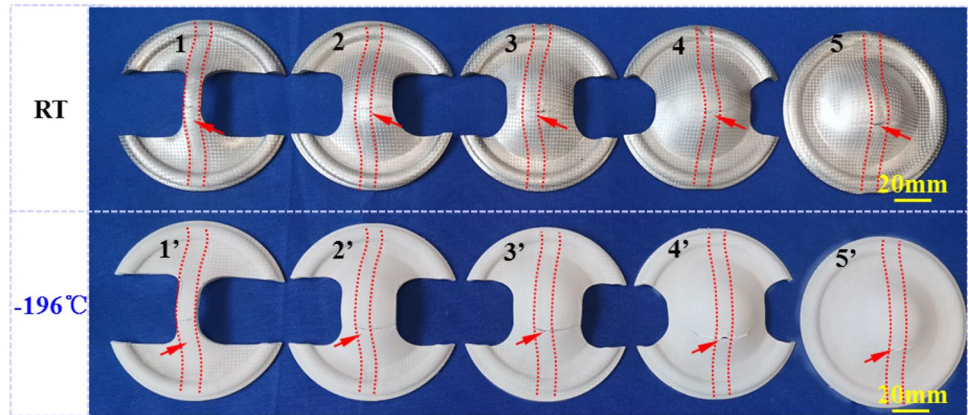
The FLCs of the FSW blanks

Figure 9 shows formed samples after failure by the Naka-jima tests. The results show that the fracture positions of the bulged specimens under different strain states at RT and −196 °C all located at the weld zone, and the crack direction was perpendicular to the weld direction. This is mainly due to the fact that the major strain direction was the same as that of the welding direction during the bulging process. Compared with that of the BM zone, the strength of the weld zone increased due to friction stir processing, resulting that the plasticity was reduced.

Figure 10 shows the FLC of the FSW blanks obtained from the Nakajima experiments and the theoretical calculated results based on the mechanical properties of BM and the LW zone at different conditions. At -196 °C, the forming limit of FSW blanks was significantly improved. The major strain increased from 0.21 to 0.32 under uniaxial tension, and the minor strain changed from −0.06 to -0.04. The major strain increased from 0.17 to 0.26 under plane strain state, and the minor strain increased from 0.03 to 0.04. The major strain increased from 0.22 to 0.33 under biaxial tension state, and the minor strain increased from 0.09 to 0.12. When $f_0 = 0.97$, the theoretical FLC based on the weld zone was in good agreement with that of the experimental results, and the FLD_0 increased from 0.16 to 0.27, an increase of 68.8%. The theoretical FLC based of the BM zone by the Hill'48-MK model has a large deviation from the experimental results as shown in Table 4. At -196 °C, the theoretical forming limits of the weld zone and the BM zone
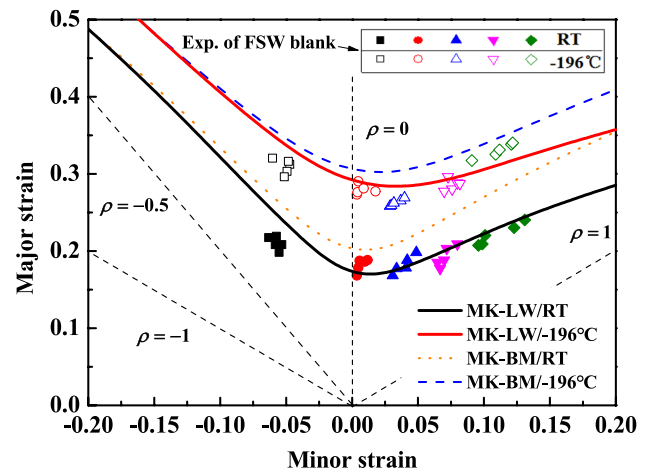

Fig. 10 Comparisons between experimental and theoretical FLCs calculated by BM and LW zone

were all improved, and the FLC of the BM zone was always above that of the weld zone, indicating that the formability of the BM zone was higher than that of the weld zone both at RT and −196 °C. The ultimate fracture strain of bulged parts under biaxial tension located between the FLC of weld zone and BM zone, which mainly resulted from the significant increase in the proportion of the BM zone for the FSW blanks. The increased effects of the BM zone on the fracture strain resulted in a decrease in the prediction accuracy of the FLC based on the weld zone. The differences in FLC based the weld and BM zone decreased at -196 °C, especially

Table 4 The errors of experimental and calculated major strain for different type specimen

Specimen width		Exp.	Cal. by LW zone	Cal. by BM zone	Error (=Cal.-Exp.)
10 mm	1	0.21	0.23	0.26	0.02/0.05
	1'	0.32	0.33	0.34	0.01/0.02
30 mm	2	0.17	0.17	0.20	0.00/0.03
	2'	0.26	0.29	0.30	0.03/0.04
40 mm	3	0.19	0.18	0.22	-0.01/0.04
	3'	0.26	0.28	0.31	0.02/0.05
60 mm	4	0.20	0.21	0.25	0.01/0.05
	4'	0.28	0.29	0.32	0.01/0.04
100 mm	5	0.22	0.24	0.29	0.02/0.07
	5'	0.33	0.30	0.34	-0.03/0.01

in the biaxial tension state, which was mainly due to the reduced strength differences between the weld and BM zone.

The LDR of the FSW blanks

Figure 11 shows that the cups height and LDR of the FSW blanks at low temperature increased significantly. The LDR at RT was 1.80, and the LDR at -160 °C and − 196 °C were 1.88 and 1.90, which increased by 4.4% and 5.6%, respectively. The cups height at -196 °C reached 94.3 mm with an increase of 14.4% compared with 82.4 mm at RT. It can be observed that the failure occurred at the suspended area of the hemispherical bottom in the weld zone of the partially drawn cup at RT and − 196 °C. The crack direction was perpendicular to the weld direction. The results show that the cryogenic formability of FSW blanks was enhanced in complex stress conditions. The formability of weld zone was significantly affected by its cryogenic mechanical properties. The uniform deformation ability of weld zone was improved at ultra-low temperature, which contributed to the enhanced formability of FSW blank.

Fracture prediction of the deep-drawn parts

Figure 12 shows the strain paths at different positions in the weld zone during the deep drawing process of the hemispherical bottom cylindrical part when the initial blank diameter D_0 was 190 mm. In Fig. 12a, the circumferential compressive strain at P1 is much larger than the tensile strain, P2 is in a pure shear state ($\rho=-1$), P3 is in a uniaxial tension state ($\rho=-0.5$), P4 is an approximate state of the plane strain state ($\rho=0$), and the position of P5 at the top of the part is in a biaxial tension state ($\rho=1$). During RT deep drawing, the P4 exceeded the FLC_0 in the weld zone, and there is a tendency to crack at this position. The strain at other locations was in the safe area below the FLC. At -196 °C, as shown in Fig. 12b, qualified drawn

Fig. 11 The cups height (**a**) and LDR (**b**) of the FSW blanks and experimental deep drawn cups obtained from different initial blank diameters at RT and − 196 °C
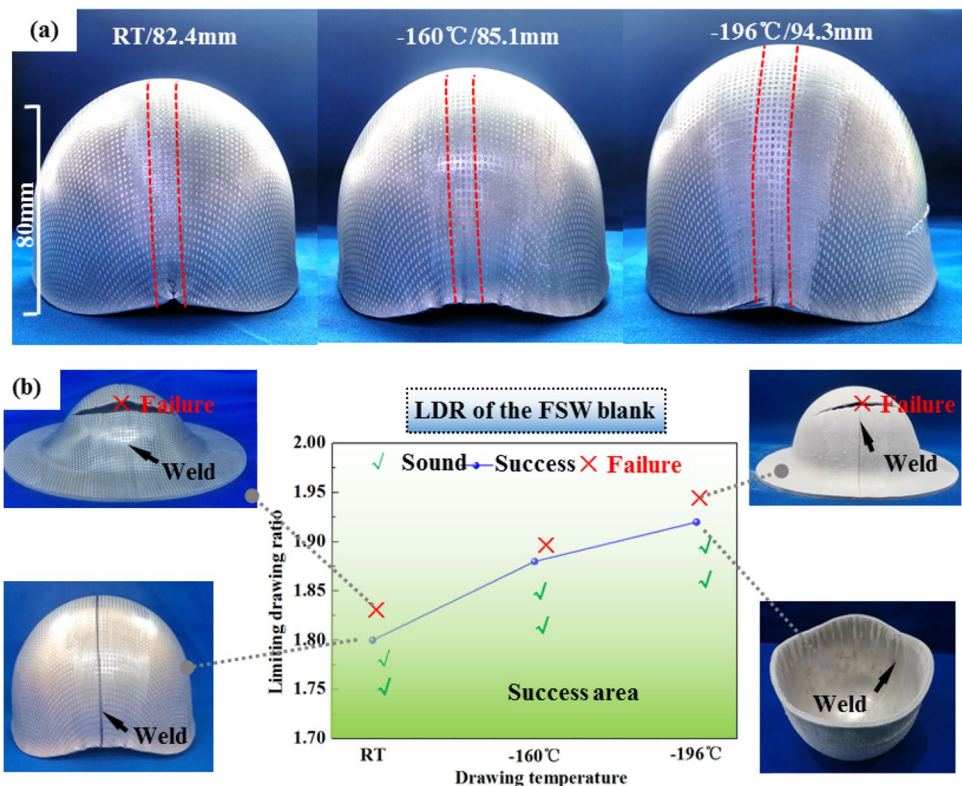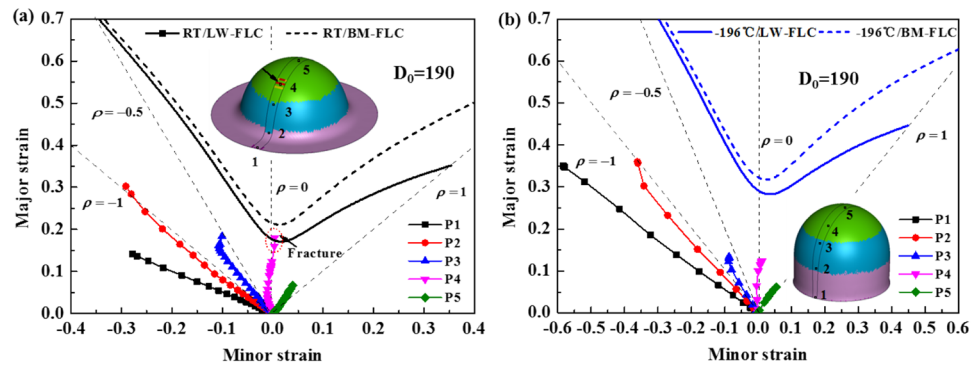
Fig. 12 Strain paths at different positions of weld zone for deep-drawn parts at RT (**a**) and − 196 °C (**b**)

parts were obtained. It was found that this was mainly due to the increase of the forming limits in the weld zone and the changed strain paths at different positions during cryogenic drawing process. The maximum major strain at P4 in the plane strain state decreased from 0.17 to 0.12 and by 29.4%. Because of the improved uniform deformation ability of the weld zone at the hemispheric bottom, the cracking did not occur at P4 in the process of large strain of the cylinder wall. The hyper hardening and high plasticity at cryogenic temperatures can make the weld zone stronger. The cryogenic deformation change the comparatively weak zones. The weaker zone will become stronger after deformation because of cryogenic hardening. Therefore, the deformation can withstood and transferred so as to avoid the strain localization. The FLC level increased obviously at cryogenic temperatures. The excessive thinning of the hemispherical bottom cylindrical part did not occur, and the tensile instability of the P4 was suppressed. Therefore, the strain was smaller at -196 °C. At the same time, the strain of P1 and P2 subjected hoop compressive stress increased at ultra-low temperature.

Figure 13 shows the strain paths at different positions of the weld zone during − 196 °C deep drawing for the hemispheric bottom cylindrical part when the initial blank diameter D_0 was 200 mm. The initial blank diameter increased to 200 mm, which exceed the cryogenic LDR of the FSW blank, the cracks occurred in the weld zone that was consistent with that of the experimental results. The major strain at P4 reached the ultimate fracture strain of the weld zone, and cracking occurred. The fracture strain at P3, P4 and P5 were also improved due to the increased cryogenic forming limits in the weld zone. In summary, the increase of the LDR under cryogenic temperature conditions was mainly due to the significant increase in the forming limit of the weld zone, especially in the plane strain state. The significantly increased cryogenic ductile fracture characteristics postponed the instability and contributed to the improvement of cryogenic forming limits [37].
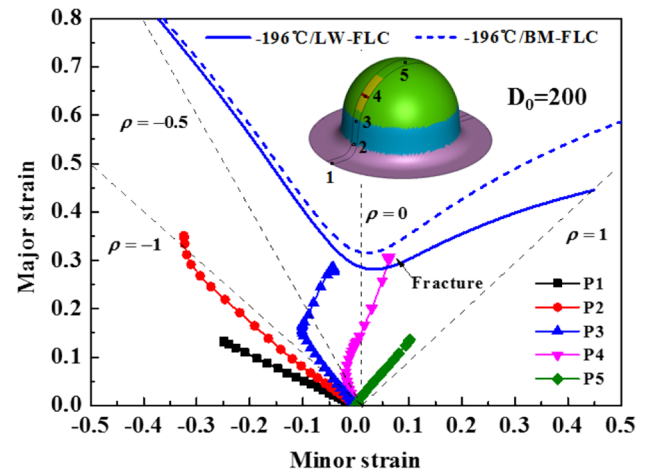

Fig. 13 Strain paths of different positions in the weld zone for deep drawing part when the initial blank diameter D_0 was 200 mm at -196 °C

Prediction on cryogenic formability

Effect of blank holder force on cryogenic formability

Figure 14 shows the effect of blank holder force on the cryogenic deep drawing of FSW blanks. The safety margin was 5%, which was the range below the FLC. When the thickness-diameter ratio was 10.5‰, the drawing height was 87.8 mm with the blank holder force of 2kN, and the flange area was seriously wrinkled. When the blank holder force was 5kN, the flange area was not wrinkled, but the straight wall of part was seriously wrinkled due to the circumferential compression. The blank holder force increased to 10kN, the wrinkling of the straight wall was obviously relieved, and the deep-drawn part height was 92.4 mm. The blank holder force was 15kN, the wrinkling in the straight wall area was eliminated, and the drawing height reached 96.3 mm. The deep-drawn part cracked at the weld position of the suspended area when the blank holder force was 20kN. Therefore, the wrinkling defects of flange area and

Fig. 14 Cryogenic formability of hemispheric bottom cylindrical parts under different blank holder forces that the thickness-diameter ratio was 10.5‰
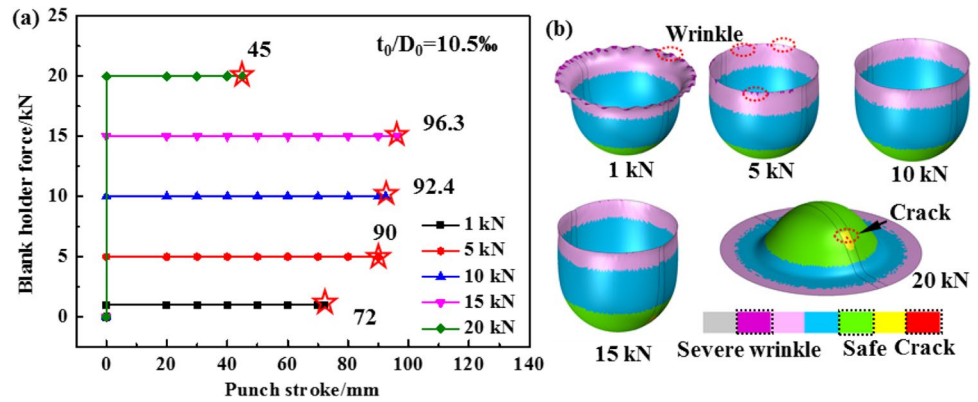
straight wall for the cryogenic drawn parts with thickness-diameter ratio of 10.5‰ can be eliminated by increasing the blank holder force, and the critical blank holder force can be used as 15kN. The higher cryogenic hardening lead to withstand and transfer deformation and prevent localized deformation from weld splitting. The radial tensile stress can be increased to reduce the circular compressive stress finally [6].

Effect of cryogenic temperature on formability

Figure 15 analyzes the effect of deformation temperature for weld and BM zone on the deep-drawn part with thickness-diameter ratio of 10.5‰. A fixed blank holder gap of 2.2 mm was adopted during the deep drawing process. Figure 15a shows that the deep-drawn part height was 67 mm at RT. The weld zone cracked at the suspended area of the part. The strain evolution was analyzed during deep drawing for point "A" of weld zone and point "B" of BM zone at the same latitude of fracture location. At RT, the maximum major strain exceed the forming limits of the weld zone at point "A". However, for the point "B", due to the larger fracture strain and the strain offset to biaxial tension, the BM zone did not reach to ultimate fracture strain and the splitting did not occur.

When the BM and weld zone were at RT and − 196 °C, respectively, the blank was in a differential temperature state. The splitting occurred in BM zone of suspended area when the deep-drawn part height was 69.1 mm as shown in Fig. 15b. The major strain of BM zone firstly reached to the forming limits in plane strain state. Plane strain cracking occurred in the BM zone. For the weld zone, the uniform deformation ability was improved at -196 °C. The hyper hardening will help to withstand and transfer deformation, and inhibit cracking caused by deformation localization. Significantly strain drift also occurred in the weld zone, and the formability was higher than that of the BM zone.

When the weld zone and the BM zone were at -196 °C, a qualified cylindrical part with a height of 90.5 mm can be obtained as shown in Fig. 15c, and the strain distribution between the weld and the BM zone was more uniform. At ultra-low temperature, the strain path differences of the weld and BM zone were smaller, indicating a significant improvement in deformation uniformity. The hardening and plasticity of the weld zone and BM zone were significantly improved at ultra-low temperature. The strength difference reduced at the same time, and the strain difference reduced finally. In addition, the hyper hardening strengthen the weak deformation zone, and the strengthening weak zone at the bottom of cylindrical part was conducive to the deformation transmission and achieve uniform deformation.

Effect of weld locations

Figure 16 shows the cryogenic formability and the FLCs of the BM and weld zone during cryogenic deep drawing with different blank diameters. The center line of weld deviated from the blank center by 48 mm. The results show that the qualified part was obtained with the blank diameter of 190 mm, and the weld zone was in the tension-compression state other than the plane strain and the biaxial tension zone. The formability of the weld zone was improved. Although the weld cracked at the weld zone located in the center of FSW blanks with the diameter of 195 mm, a qualified deep-drawn part can be obtained with the offset weld. When the blank was 200 mm, the deep-drawn part cracked in the BM zone, and the crack was located in the transition area between the BM zone and the weld zone. The weld zone was in the safe zone of the FLC, which was obviously different from that of the deep drawing with the central weld. In conclusion, the strain state of weld zone changed during cryogenic deep drawing process, and the weld zone of the FSW blank with offset weld was in a tension-compression state. Compared with that of intermediate weld blank, the cryogenic deep drawing properties of FSW blanks was further improved. The formability was found to be dependent on the

Fig. 15 Formability of FSW blank of hemispherical bottom cylindrical parts at different temperatures
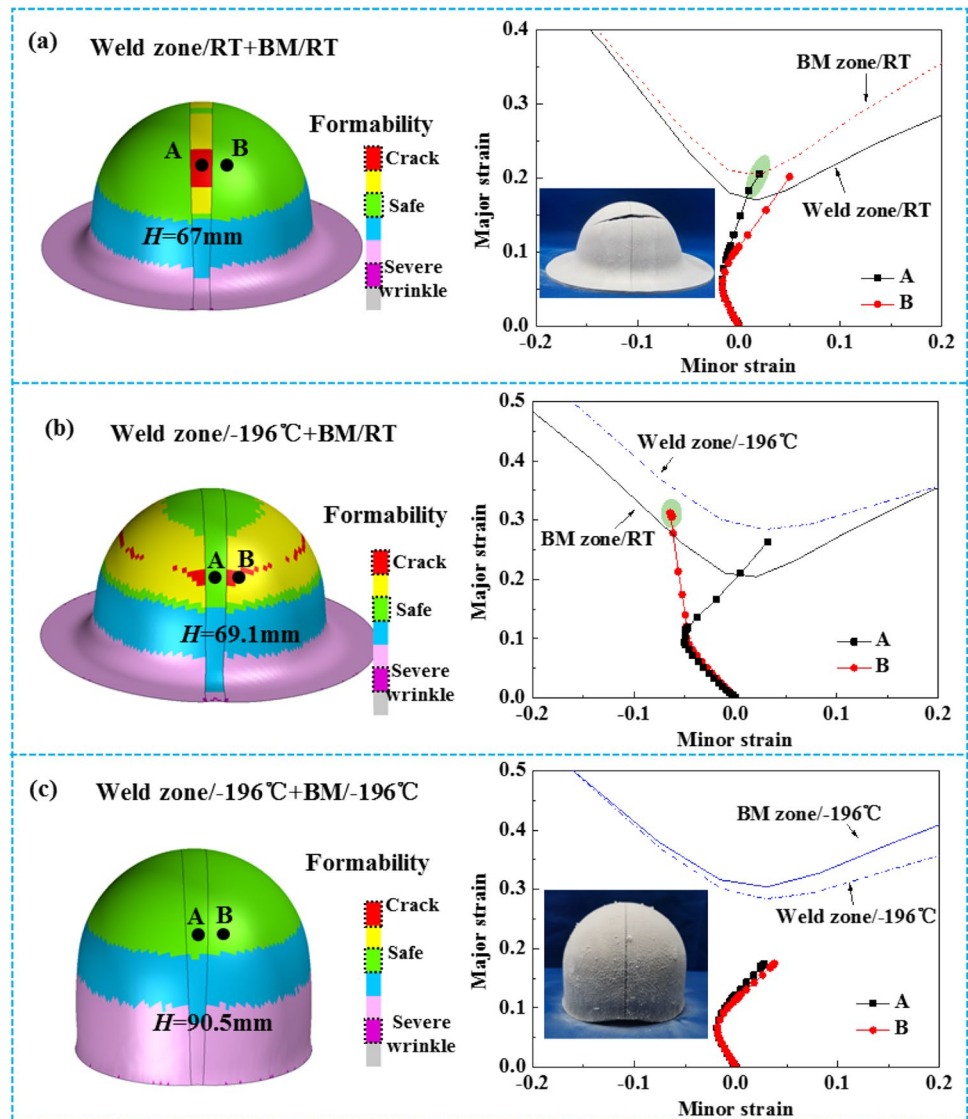
weld line position, and the formability increased when the weld was located farther from the blank center due to more uniform strain [38].

Failure mode analysis

Figure 17 shows the failure mode analysis of FSW blanks during cryogenic deep drawing. The splitting occurred at the weld position in unsupported wall region (white circles) of the drawn part during isothermal deep drawing, and the splitting direction was perpendicular to the weld direction. However, splitting occurred in the BM zone near the weld during differential temperature deep drawing. The strength and plasticity of weld zone and BM zone were different obviously [24]. The splitting was caused by excessive deformation of the BM zone, and the flow stress reached the ultimate strength. However, the hyper hardening of weld zone lead to increased formability of the weld zone. Also, in cryogenic deep drawing of blanks with offset weld, cracks occurred near the weld due to the low plasticity of BM zone, and the crack direction was parallel to the weld direction. In addition, according to the strain evolution, it is found that the splitting of isothermal and non-isothermal deep drawing depend on the ultimate fracture strain of weak zone with low plasticity. The former was determined by the weld zone with poor plasticity, while the latter depend on the plasticity of BM zone at RT. The deformation uniformity between weld and BM zone can be improved during isothermal deep drawing. Moreover, the offset weld contributed to improve the cryogenic formability due to the changed strain path of the weld

Fig. 16 Cryogenic formability of hemispherical bottom cylindrical parts of FSW blanks with offset welds and different initial blank diameters
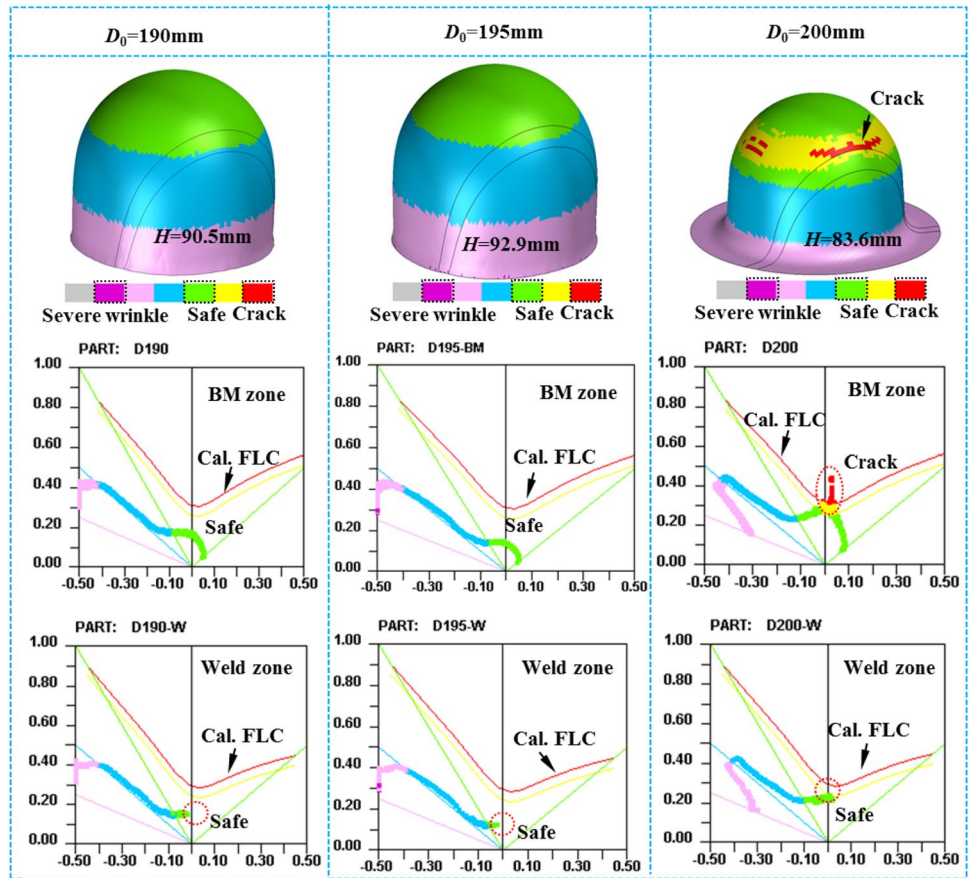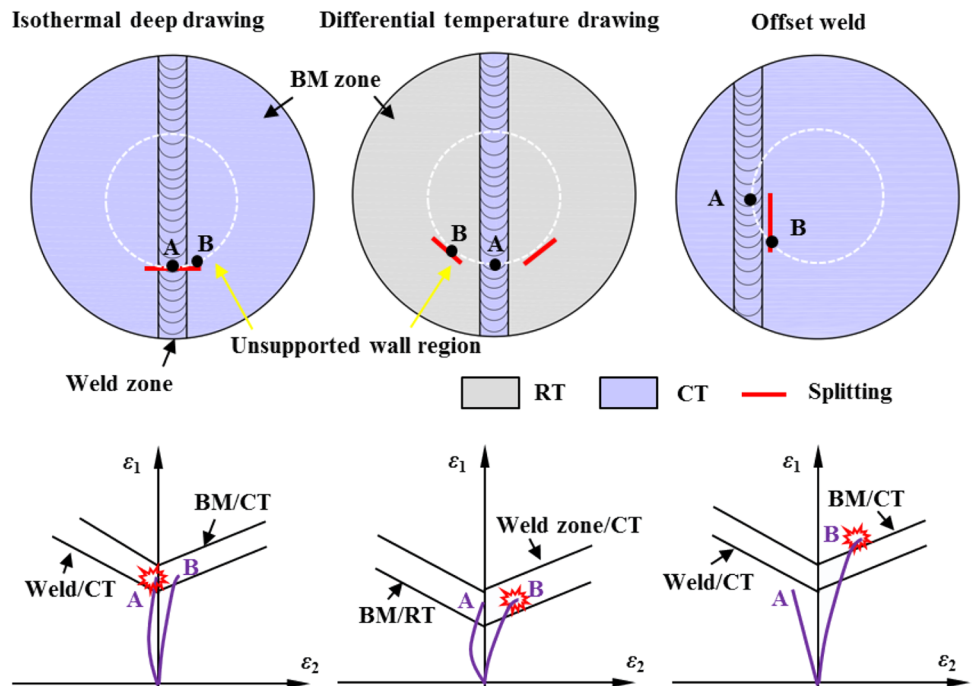

Fig. 17 Schematic of failure modes for FSW blanks with different cryogenic forming process

zone [39, 40], and the splitting occurred in the BM zone with hyper hardening and excellent plasticity at cryogenic temperatures.

According to above simulative analysis based on the theoretical FLCs, the following ways were proposed to improve the cryogenic formability of FSW blanks: (i) Under the ultra-low temperature, the strength and plasticity of the weld and BM zone both increased, and the ultimate fracture strain of the cylindrical part increased. By increasing the blank holder force, qualified deep-drawn parts can be formed, and at the same time, the wrinkling of the flange area and the straight wall can be effectively suppressed. The hyper hardening and high plasticity of the weak zone indicated that deformation can be transferred with increased blank holder force. (ii) Cryogenic deformation uniformity of the FSW blanks was improved during isothermal deep drawing. The decreased strength differences between the weld zone and BM zone help to the decreased strain difference at ultra-low temperatures. (iii) The strain state of the weld zone also can be changed by offset weld at ultra-low temperature. Shifting the initial weld line position contributed to the improved formability, which was validated through deep drawing experiments [41]. The increased weld zone fracture strain further contributed to the improved deep drawing properties of the FSW blank. The above results based on the theoretical FLCs provided technical supports for the subsequent cryogenic deep drawing of large thin-walled curved parts of Al alloys FSW blanks.

Conclusion

In this paper, the mechanical properties of 2219-O aluminum alloy FSW blanks were studied at -196 °C. The FLCs and the LDR of the hemispherical bottom cylindrical part were obtained by the experiments at different conditions. The theoretical FLC can accurately predict the cryogenic deep drawing splitting behavior of the drawn part. The effective methods were proposed to improve cryogenic formability of FSW blanks. The main conclusions are as follows:

(1) At ultra-low temperatures, the strength and plasticity of the weld and BM zone both increased. The elongation and hardening exponent of the weld zone at -196 °C were 28.5% and 0.44, which were 30.7% and 51.7% higher than that at RT, respectively.

(2) The cryogenic forming limit of FSW blanks increased significantly, and the FLD_0 increased from 0.16 at RT to 0.27 at -196 °C. The theoretical FLC calculated based on the M-K model was in good agreement with the experimental results.

(3) The LDR of the hemispherical bottom cylindrical part reached 1.90 at -196 °C. The fracture position of the drawn part was located at the weld of the hemispherical bottom suspended area, and the direction of the splitting was perpendicular to the weld direction. The established FLC and the M-K theoretical model can accurately predict the splitting behavior.

(4) The hyper hardening and high plasticity of the FSW blank indicated that deformation can be transferred with increased blank holder force at ultra-low temperatures. The problems of wrinkling and splitting all can be overcoming. The strain distribution between the weld and BM zone was more uniform by using isothermal deep drawing. The cryogenic formability of FSW blanks was further improved with offset weld.

In this paper, the influence of ultra-low temperatures on the forming mechanism and formability of thin-wall hemispherical part were studied. However, the present results still need to be improved such as the effect of differential temperature on formability of the FSW blanks, which need to be verified for the large size thin-wall components during cryogenic deep drawing. In addition, the theoretical analysis of the reasons for the improvement of cryogenic formability are need to be further carried out, and the effect of weld locations should be elaborated at ultra-low temperatures.

Declarations

References

1. Yuan S (2021) Fundamentals and processes of fluid pressure forming technology for complex thin-walled components. Engineering 7:358–366. https://doi.org/10.1016/j.eng.2020.08.014

2. Parente M, Safdarian R, Santos AD et al (2016) A study on the formability of aluminum tailor welded blanks produced by friction stir welding. Int J Adv Manuf Technol 83:2129–2141. https://doi.org/10.1007/s00170-015-7950-0

3. Zhang H, Zhan M, Zheng Z et al (2022) Forming dependence on spin roller paths for thin-walled complex components from 2195 Al-Li alloy TWBs. Int J Adv Manuf Technol 120:3113–3122. https://doi.org/10.1007/s00170-022-08974-y

4. Carlone P, Thuillier S, Andrade-Campos A et al (2021) Incremental forming of friction-stir welded aluminium blanks: an integrated approach. Int J Mater Form 14:1121–1137. https://doi.org/10.1007/s12289-021-01628-6

5. Abbasi M, Bagheri B, Abdollahzadeh A, Moghaddam AO (2021) A different attempt to improve the formability of aluminum tailor welded blanks (TWB) produced by the FSW. Int J Mater Form 14:1189–1208. https://doi.org/10.1007/s12289-021-01632-w

6. Fan X, Yuan S (2022) Innovation for forming aluminum alloy thin shells at ultra-low temperature by the dual enhancement effect. Int J Extrem Manuf 4:033001. https://doi.org/10.1088/2631-7990/ac6b62

7. Zheng K, Politis DJ, Wang L, Lin J (2018) A review on forming techniques for manufacturing lightweight complex—shaped aluminium panel components. Int J Light Mater Manuf 1:55–80. https://doi.org/10.1016/j.ijlmm.2018.03.006

8. Grabner F, Gruber B, Schlögl C, Chimani C (2018) Cryogenic sheet metal forming - An overview. Mater Sci Forum 941:1397–1403. https://doi.org/10.4028/www.scientific.net/MSF.941.1397

9. Zhang R, Shao Z, Lin J (2018) A review on modelling techniques for formability prediction of sheet metal forming. Int J Light Mater Manuf 1:115–125. https://doi.org/10.1016/j.ijlmm.2018.06.003

10. Ghoo BY, Park SW, Keum YT (2001) New forming limit diagram of laser tailored blank. J Strain Anal Eng Des 36:143–152. https://doi.org/10.1243/0309324011512694

11. Kumar G, Maji K (2022) Forming limit analysis of friction stir tailor welded AA5083 and AA7075 sheets in single point incremental forming. Int J Mater Form 15. https://doi.org/10.1007/s12289-022-01675-7

12. Zadpoor AA, Sinke J, Benedictus R (2008) Theoretical prediction of failure in forming of friction stir welded blanks. Int J Mater Form 1:305–308. https://doi.org/10.1007/s12289-008-0341-4

13. Kobayashi M, Kamada A, Terabayashi T, Asao H (1980) Press formability of face-centred cubic metals at cryogenic temperatures BT - Proceedings of the twentieth international machine tool design and research conference: Sub-conference on electrical processes. In: Tobias SA (ed). Palgrave Macmillan UK, London, pp 239–246

14. Wang C, Yi Y, Huang S et al (2021) Experimental and theoretical investigation on the forming limit of 2024-O aluminum alloy sheet at cryogenic temperatures. Met Mater Int 27:5199–5211. https://doi.org/10.1007/s12540-020-00922-3

15. Yuan S, Cheng W, Liu W (2021) Cryogenic formability of a solution-treated aluminum alloy sheet at low temperatures. J Mater Process Technol 298:117295. https://doi.org/10.1016/j.jmatprotec.2021.117295

16. Yuan S, Cheng W, Liu W, Xu Y (2020) A novel deep drawing process for aluminum alloy sheets at cryogenic temperatures. J Mater Process Technol 284:116743. https://doi.org/10.1016/j.jmatprotec.2020.116743

17. Schneider R, Grant RJ, Schlosser JM et al (2020) An investigation of the deep drawing behavior of automotive aluminum alloys at very low temperatures. Metall Mater Trans A 51:1123–1133. https://doi.org/10.1007/s11661-019-05584-4

18. Zadpoor AA, Sinke J, Benedictus R (2007) Mechanics of tailor welded blanks: An overview. Key Eng Mater 344:373–382

19. Bressan JD, Bruschi S, Ghiotti A (2016) Prediction of limit strains in hot forming of aluminium alloy sheets. Int J Mech Sci 115–116:702–710. https://doi.org/10.1016/j.ijmecsci.2016.07.040

20. Wang H, Yan Y, Han F, Wan M (2017) Experimental and theoretical investigations of the forming limit of 5754O aluminum alloy sheet under different combined loading paths. Int J Mech Sci 133:147–166. https://doi.org/10.1016/j.ijmecsci.2017.08.040

21. Li Z, Zhou G, Li D et al (2020) Forming limits of magnesium alloy AZ31B sheet at elevated temperatures. Int J Plast 135:102822. https://doi.org/10.1016/j.ijplas.2020.102822

22. Xiang N, Wang Z, Cai S (2018) Mechanism on increased sheet formability induced by tangential adhesive stress in sheet flexible forming process employing viscoplastic pressure-carrying medium. Int J Mach Tools Manuf 133:18–30. https://doi.org/10.1016/j.ijmachtools.2018.04.008

23. Chung K, Lee W, Kim D et al (2010) Macro-performance evaluation of friction stir welded automotive tailor-welded blank sheets: Part I - Material properties. Int J Solids Struct 47:1048–1062. https://doi.org/10.1016/j.ijsolstr.2009.12.022

24. Lee W, Chung KH, Kim D et al (2009) Experimental and numerical study on formability of friction stir welded TWB sheets based on hemispherical dome stretch tests. Int J Plast 25:1626–1654. https://doi.org/10.1016/j.ijplas.2008.08.005

25. Ramulu PJ, Narayanan RG (2011) Predicting the forming limit of friction stir welded blanks. AIP Conf Proc 1353:219–223. https://doi.org/10.1063/1.3589518

26. Ramulu PJ, Narayanan RG (2013) Experimental evaluation and prediction of forming limit of FSW blanks made of AA 6061 T6 sheets at different weld orientations and weld locations. Materwiss Werksttech 44:527–540. https://doi.org/10.1002/mawe.201300078

27. Cheng CH, Chan LC, Chow CL (2004) Experimental investigation on the weldability and forming behavior of aluminum alloy tailor-welded blanks. PICALO 2004–1st Pacific Int Conf Appl Laser. Opt Conf Proc 81:19–24. https://doi.org/10.2351/1.5056100

28. Saunders FI, Wagoner RH (1996) Forming of tailor-welded blanks. Metall Mater Trans A 27:2605–2616. https://doi.org/10.1007/BF02652354

29. Bandyopadhyay K, Basak S, Panda SK, Saha P (2015) Use of stress based forming limit diagram to predict formability in two-stage forming of tailor welded blanks. Mater Des 67:558–570. https://doi.org/10.1016/j.matdes.2014.10.089

30. Banabic D, Kami A, Comsa DS, Eyckens P (2021) Developments of the Marciniak-Kuczynski model for sheet metal formability: A review. J Mater Process Technol 287:116446. https://doi.org/10.1016/j.jmatprotec.2019.116446

31. Marciniak Z, Kuczyński K (1967) Limit strains in the processes of stretch-forming sheet metal. Int J Mech Sci 9:609–620. https://doi.org/10.1016/0020-7403(67)90066-5

32. Bleaney B, Penrose RP, Plumpton BI (1949) The theory of plane plastic strain for anisotropic metals. Proc R Soc London Ser A Math Phys Sci 198:428–437. https://doi.org/10.1098/rspa.1949.0110

33. Cheng W, Liu W, Yuan S (2019) Deformation behavior of Al–Cu–Mn alloy sheets under biaxial stress at cryogenic temperatures. Mater Sci Eng A 759:357–367. https://doi.org/10.1016/j.msea.2019.05.047

34. Cerri E, Leo P (2010) Warm and room temperature deformation of friction stir welded thin aluminium sheets. Mater Des 31:1392–1402. https://doi.org/10.1016/j.matdes.2009.08.044

35. Aydin H, Bayram A, Uğuz A, Akay KS (2009) Tensile properties of friction stir welded joints of 2024 aluminum alloys in different heat-treated-state. Mater Des 30:2211–2221. https://doi.org/10.1016/j.matdes.2008.08.034

36. Hao Y, Liu W (2022) Analysis on exceptional cryogenic mechanical properties of AA2219 alloy FSW joints in

multi-scale. Mater Sci Eng A 850:143489. https://doi.org/10.1016/j.msea.2022.143489

37. Wang X, Fan X, Chen X, Yuan S (2022) Forming limit of 6061 aluminum alloy tube at cryogenic temperatures. J Mater Process Technol 306:117649. https://doi.org/10.1016/j.jmatprotec.2022.117649

38. Li J, Nayak SS, Biro E et al (2013) Effects of weld line position and geometry on the formability of laser welded high strength low alloy and dual-phase steel blanks. Mater Des 52:757–766. https://doi.org/10.1016/j.matdes.2013.06.021

39. Riahi M, Amini A, Sabbaghzadeh J, Torkamany MJ (2012) Analysis of weld location effect and thickness ratio on formability of tailor welded blank. Sci Technol Weld Join 17:282–287. https://doi.org/10.1179/1362171812Y.0000000005

40. Narayanan RG (2015) Formability of friction stir welded sheets made of AA 6061-T6 at different weld orientations and weld locations Perumalla Janaki Ramulu Satish Vasu Kailas. Internatioanl J Mater Prod Technol 50:147–160

41. Bandyopadhyay K, Panda SK, Saha P, Padmanabham G (2015) Limiting drawing ratio and deep drawing behavior of dual phase steel tailor welded blanks: FE simulation and experimental validation. J Mater Process Technol 217:48–64. https://doi.org/10.1016/j.jmatprotec.2014.10.022